Sympathetically cooled and compressed positron plasma

B. M. Jelenković,[1,2] A. S. Newbury,[1,*] J. J. Bollinger,[1,†] W. M. Itano,[1] and T. B. Mitchell[3]
[1]*Time and Frequency Division, National Institute of Standards and Technology, Boulder, Colorado 80303, USA*
[2]*Institute of Physics, University of Belgrade, Belgrade, Yugoslavia*
[3]*Department of Physics and Astronomy, University of Delaware, Newark, Delaware 19716, USA*
(Received 27 February 2003; published 18 June 2003)

We report sympathetic cooling and compression of a few thousand positrons by laser-cooled $^9Be^+$ ions in a Penning ion trap. The observed centrifugal separation of the two species implies approximate rigid rotation of the positrons and $^9Be^+$ ions, and a positron density comparable to the $^9Be^+$ ion density of $\gtrsim 4\times10^9$ cm^{-3}. We use the sharpness of the separation to place a 5-K upper limit on the positron temperature of motion parallel to the magnetic field. The positron lifetime is greater than two weeks in our room-temperature Penning trap.

DOI: 10.1103/PhysRevA.67.063406 PACS number(s): 32.80.Pj, 52.27.Jt

I. INTRODUCTION

Cold, dense positron plasmas in traps have wide-ranging applications in physics. Trapped positrons can be extracted and used as a source for a bright positron beam in surface science [1] and atomic physics [2,3] studies. Reservoirs of cold, dense positrons should be useful in making cold antihydrogen by passing cooled antiprotons through the trapped positrons [4,5]. Cold, dense positron plasmas are also the starting point for a number of interesting and exotic studies in plasma physics. Examples include a combined electron-positron plasma [6] and a positron plasma cooled to temperatures where the plasma crystallizes and the plasma modes must be treated quantum mechanically [7].

Much progress has been obtained over the last decade in trapping and cooling positrons [8–14]. Recent experiments by Gabrielse and by Surko and their co-workers report ''state of the art'' results in trapping dense, cold positrons. With a cryogenic Penning trap, a 110-mCi ^{22}Na source, and tungsten moderators, Gabrielse and co-workers [11,12] trapped $\sim 2\times10^6$ positrons at a density of $\sim 7\times10^6$ cm^{-3}. Surko and co-workers [13,14], using a 90-mCi positron source, a room-temperature Penning-Malmberg trap, and a solid Ne moderator, report the largest number of trapped positrons ($\sim 3\times10^8$ in 8 min). In this case, the positrons had a $\sim$300 K temperature distribution and number densities of $\sim 8\times10^7$ cm^{-3}.

This paper presents experimental results on the capture, storage, and sympathetic cooling and compression of positrons in a Penning trap containing laser-cooled $^9Be^+$ ions. Preliminary accounts of the work have been reported in Refs. [15,16]. Here we expand those discussions and summarize additional attempts to accumulate positrons after heating the moderator crystal to high temperatures. This experimental work follows simulations of trapping and sympathetic cooling of positrons via Coulomb collisions with cold $^9Be^+$ ions [17,18]. The basic idea consists of simultaneously storing positrons and $^9Be^+$ ions in the same Penning ion trap. Radiation pressure from a laser beam (i.e., Doppler laser cooling) is used to cool the $^9Be^+$ ions and apply a torque that compresses the ions to high density. Through the Coulomb interaction, the $^9Be^+$ ions and positrons exchange energy and momentum. If this exchange of energy and momentum is strong enough to overcome the ambient sources of heat and torques on the positrons, the e^+-$^9Be^+$ plasma will evolve into a global thermal equilibrium state characterized by equal temperatures and rotation frequencies of the positrons and $^9Be^+$ ions. At low temperature, this results in centrifugal separation of the species and positron densities nearly identical to the $^9Be^+$ ion densities [19].

We report here centrifugal separation of the $^9Be^+$ ions and positrons, with the positrons compressed into a narrow column along the trap's magnetic-field axis with density $\gtrsim 4\times10^9$ cm^{-3}. Centrifugal separation of two-species ion plasmas has been observed and studied in $^9Be^+$-Hg^+ [20], $^9Be^+$-$^{26}Mg^+$ [21], $^9Be^+$-Cd^+ [22], and $^9Be^+$-$^{136}Xe^{q+}$ ($32 \leqslant q \leqslant 44$) [23] plasmas. In these experiments, laser cooling one ion species resulted in temperatures of $\lesssim$0.5 K for the other ion species. However, the energy transfer in a e^+-$^9Be^+$ collision is $\sim$1000 times weaker than in these ion-ion sympathetic cooling studies. Sympathetic cooling of antiprotons by 4-K electrons in a Penning trap has been observed [12]. Also, protons have been cooled by 4-K electrons and antiprotons by 4-K positrons in nested Penning traps [12,24]. No evidence of centrifugal separation was observed in any of these experiments involving electrons or positrons. Possible reasons include insufficient densities and temperatures for separation to occur [19] or the lack of establishment of a rotational equilibrium. Centrifugal separation of the positrons and $^9Be^+$ ions enables us to determine the positron density and place a rough upper bound on the positron temperature.

In Sec. II, we describe the experimental setup and in Sec. III the positron detection methods. In Sec. IV, we present the measured accumulation rates. Our method for estimating temperature limits is discussed in Sec. V. We conclude by summarizing and discussing future possibilities.

II. EXPERIMENT

Figure 1(a) shows a schematic of the experimental setup [15]. The top (load) trap was used to create $^9Be^+$ ions by electron-beam ionizing neutral Be atoms sublimated from a heated Be filament. The $^9Be^+$ ions are then transferred to the

*Permanent address: Ball Aerospace, Boulder, CO 80301.
†Electronic address: john.bollinger@boulder.nist.gov

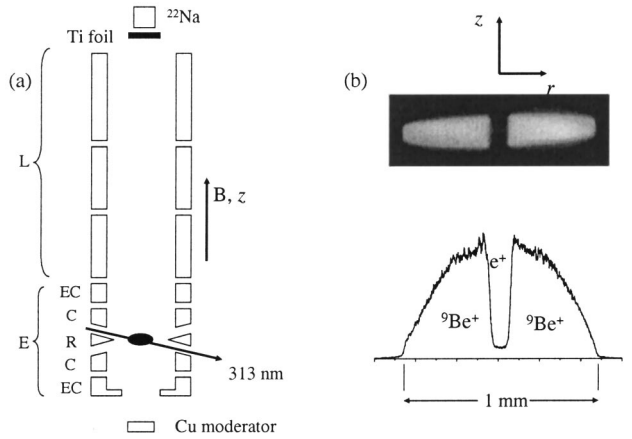

FIG. 1. (a) Schematic diagram of the load (L) and experimental (E) cylindrical Penning traps (drawn to scale); EC, end cap; C, compensation; R, ring of the experimental trap. (b) Two-species $^9Be^+$-e^+ plasma: side-view camera image (top) and radial variation of fluorescence signal integrated over z (bottom).

lower (experimental) trap. The inner diameter of the trap electrodes (except for the experimental ring electrode) is 10 mm. The traps are enclosed in a cylindrical quartz envelope that, after baking at $\sim 350\,^\circ$C, maintains a vacuum in the low 10^{-9} Pa ($\sim 10^{-11}$ Torr) range. The trap and vacuum envelope are at room temperature. The uniform magnetic field of 5.9253 T, produced by a superconducting magnet, is aligned parallel to the trap axis within 0.01° and produces a $^9Be^+$ ion cyclotron frequency $\Omega = 2\pi \times 10.2$ MHz. An axisymmetric, nearly quadratic trapping potential is generated by biasing the ring of the experimental trap to a negative voltage V_R and adjacent compensation electrodes to $V_C = 0.9 \times V_R$. For $V_R = -100$ V, and for the end cap voltage $V_{EC} = 0$, the $^9Be^+$ single-particle axial frequency is $\omega_z = 2\pi \times 870$ kHz, and the magnetron frequency is $\omega_m = 2\pi \times 35$ kHz.

In Penning traps, an ion plasma undergoes an $\mathbf{E} \times \mathbf{B}$ drift that is a rotation about the trap symmetry axis. This rotation through the magnetic field produces, through the Lorentz force, the radial binding force of the trap and radial plasma confinement. When a plasma reaches thermal equilibrium, the entire ion plasma rotates at a uniform rotation frequency ω_r. In this experiment, laser radiation pressure as well as a rotating electric field were used to set ω_r [25,26]. The rotating electric field was generated by applying 180° out-of-phase sinusoidal potentials to two segments of a split electrode located between the ring and the lower compensation electrode (not shown in Fig. 1). The oscillating field that results is the superposition of components that rotate with and against the plasma rotation. The corotating component was used to control the plasma rotation frequency (the ''rotating wall'') [26].

The ions were cooled by a laser beam (~ 50 μm waist) tuned to near resonance with the $2s^2S_{1/2} \rightarrow 2p^2P_{3/2}$ $^9Be^+$ transition at 313 nm. The laser enters the trap at an angle of 11° with respect to the plane that is perpendicular to the magnetic field and contains the trap center ($z = 0$ plane). Based on measurements from previous experiments [27], we expect $T_\perp(Be^+) \leqslant T_\parallel(Be^+) \leqslant 100$ mK, where $T_\perp(Be^+)$ and $T_\parallel(Be^+)$ are the temperatures of the $^9Be^+$ velocity distributions in the directions perpendicular and parallel to the magnetic-field axis (z axis). The ion resonance fluorescence which was scattered approximately perpendicular to the laser beam and the magnetic field was imaged by an $f/5$ objective onto the photocathode of a photon-counting imaging detector. By a continuous translation of the cooling beam parallel to the z axis, we could illuminate a slice of the plasma containing the z axis of the trap. In this way, we were able to obtain an approximate side-view image of the $^9Be^+$ plasma as shown in Fig. 1(b).

The positrons are emitted from a 2-mCi ^{22}Na source with an active diameter of ~ 1 mm. The source is placed just above the vacuum envelope, and positrons enter the vacuum envelope through a Ti foil of ~ 7 μm thickness. Positrons travel along the axis of the Penning traps until they hit the Cu(111) moderator crystal. Moderated positrons then reenter the trap where they can be trapped and sympathetically cooled by the laser-cooled $^9Be^+$ ions. We chose a Cu(111) moderator crystal because of the expected narrow energy distribution of moderated positrons [28,29], and because it can be annealed and cleaned at a relatively modest temperature ($\sim 900\,^\circ$C).

III. POSITRON DETECTION

Trapped positrons were detected and their number measured through observations of centrifugal separation and through the annihilation radiation measured after ejecting the accumulated positrons onto the Ti foil above the trap. We start this section by discussing centrifugal separation.

If charged atomic particles with different charge-to-mass ratios rotate about the trap axis at the same radius, they will tend to rotate with different rates because of different centrifugal forces. If the particles have the same charge (for example, singly charged ions or atomic particles), the heavier particles will rotate faster than the lighter particles. Collisional drag will then cause a radial drift of the lighter ions inward, and the heavier ions outward. Centrifugal separation continues until an equilibrium is reached with both species rotating with the same ω_r [19]. In the $T \rightarrow 0$ limit, the separation is complete and the density of either species is determined by the rotation frequency, $n_i = 2\epsilon_0 M_i \omega_r (\Omega_i - \omega_r)/q_i^2$ [19]. Here n_i, M_i, Ω_i, and q_i are the density, mass, cyclotron frequency, and charge of the ith species. If $q_1 = q_2$ and $\omega_r \ll \Omega_1, \Omega_2$, then the densities are approximately equal and the combined shape of the plasma is a spheroid. Therefore trapped positrons, if cooled to low temperatures, will move to orbital radii smaller than those for the $^9Be^+$ ions, with the positrons forming a column of uniform density along the trap axis.

Figure 1(b) shows a side-view image of a $^9Be^+$ plasma and the corresponding radial dependence of the $^9Be^+$ fluorescence after accumulating positrons for many hours. The ''dark'' nonfluorescing column in the plasma is due to the presence of particles with charge-to-mass ratio greater than that of $^9Be^+$. We determined that most ($>95\%$) of this column is due to positrons from the lifetime of this column

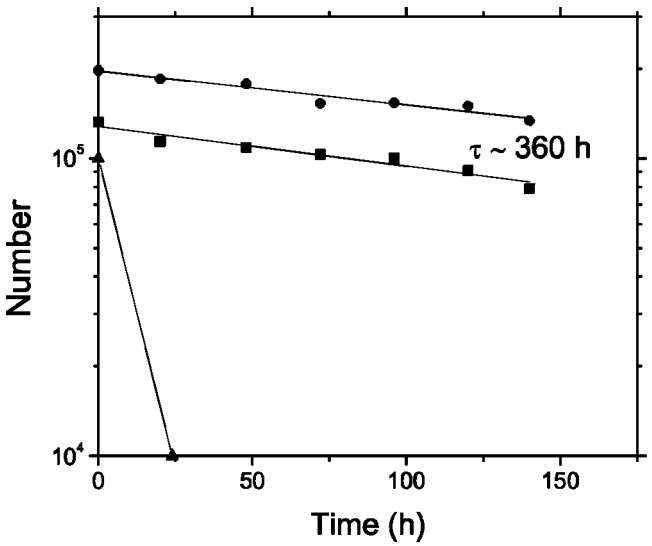

FIG. 2. Number of trapped positrons (solid circles, number shown is equal to actual number multiplied by 100), $^9Be^+$ ions (solid boxes) and light impurity ions (triangles) as a function of time after they are created.

after the ^{22}Na was blocked. By multiplying the positron density ($\omega_r = 2\pi \times 450$ kHz, $n_{e^+} \simeq n_{Be^+} \simeq 1.8 \times 10^9$ cm^{-3}) with the observed volume of the nonfluorescing column (diameter $= 1.0 \times 10^{-2}$ cm, length $= 1.6 \times 10^{-2}$ cm), we estimate that 2000 cold positrons are present in the plasma.

The lifetime of the nonfluorescing column in Fig. 1(b) was determined by blocking the ^{22}Na source and measuring the decrease in the volume of this column over a period of one week. The measured $1/e$ lifetime of the light-mass charges that make up this column was $\sim$360 h and is nearly identical to the observed $^9Be^+$ trapping lifetime [30]. In a separate experiment we measured the lifetime of impurity ions of light mass (e.g., H_2^+), which could be created and trapped while loading positrons. We deliberately created light ions (in a pure $^9Be^+$ plasma) by ionizing background molecules with a $\sim$20 eV electron beam. (The ^{22}Na source was blocked during this measurement.) Due to reactions with background gas molecules, these light-mass ions disappeared with a $1/e$ lifetime of $\sim$10 h. The 5% change in the volume of the dark central column in Fig. 1(b) after the ^{22}Na source was blocked for 20 h indicates that greater than 95% of this column is due to positrons. Figure 2 shows the measured lifetime of the positrons, $^9Be^+$ ions, and light-mass impurity ions.

The nearly identical lifetimes of the $^9Be^+$ ions and the positrons indicates that these lifetimes are likely limited by the same effect. One possibility is charged particle loss due to a slow radial expansion of the plasma between the daily measurements when the $^9Be^+$ ions (and therefore positrons) were not compressed radially by a laser beam or a rotating electric field. If the positron lifetime was limited by a trap effect like this, then the positron annihilation lifetime could be greater than 360 h. Surko and co-workers [31] measured a lifetime of $\sim$1 h in a room-temperature trap with a base pressure of $\sim 7 \times 10^{-8}$ Pa (5×10^{-10} Torr). The 360 h lifetime in our room-temperature trap, where the base pressure is possibly 50 times improved, compares very favorably with this lifetime. Our trap was baked at $\sim$350 °C for one week which should have been effective at removing large molecules which have anomalously large cross sections for positron annihilation [3].

The positrons were also directly detected by ejecting the e^+-$^9Be^+$ plasma onto the 7-μm Ti foil located above the trap. With the energy (<1 keV) that the positrons acquired while being ejected out of the trap, all the positrons annihilated in the Ti foil. The resulting annihilation radiation was detected with a NaI scintillation crystal mounted 2.5 or 5 cm above the Ti foil. A light pipe coupled the output of the NaI crystal to a photomultiplier tube mounted $\sim$0.5 m above the magnet. (The ^{22}Na source was removed from the magnet bore during this procedure.) We attempted to eject all the positrons in a period of time small compared to the rise time of the NaI crystal scintillation ($\sim$300 ns). In this way the scintillation crystal will produce a single pulse, free from background radiation, whose height is proportional to the number of annihilated positrons.

Positrons were ejected with different sets of voltages on the trap electrodes and with different pulse voltages. For example, starting with the e^+-$^9Be^+$ plasma trapped with axially symmetric voltages on the experimental trap, the experimental and load trap voltages were adiabatically changed so that the e^+-$^9Be^+$ plasma was moved to the region of the lower end cap of the load trap, where it was confined by the following electrode potentials: 900 V, 900 V, 900 V, 850 V, 800 V, 0 V, 250 V, and 100 V. Here the potentials are listed starting with the lower end cap of the experimental trap and moving up [see Fig. 1(a)]. The lower end cap of the load trap was then pulsed from 0 V to 500 V by a voltage pulser with a $\sim$50 ns rise time. The resulting output pulse of the photomultiplier preamplifier was recorded on a digital oscilloscope.

For a fixed procedure for positron ejection, the voltage peak of the photomultiplier annihilation pulse was proportional to the volume of the dark central column measured from side-view images such as Fig. 1(b). However, changing the electrode potentials and pulse voltages of this procedure produced, in many cases, a different proportionality constant. For some conditions the photomultiplier annihilation pulse was significantly longer than the scintillator single-event pulse and delayed beyond the scintillator and high-voltage pulse rise times. This indicated that for these conditions not all the positrons were ejected simultaneously. Presumably the reason for this is pickup and ringing induced by the high-voltage pulse on different trap electrodes. We could not detect ringing and pickup sufficient to cause this problem. However, the trap potentials could be monitored only outside the vacuum system. To estimate the number of trapped positrons, only annihilation procedures that produced single-event pulses were used.

The NaI crystal detection system was calibrated with a 32.9 kBq (~ 1 μCi) ^{68}Ge source. This is a good source for calibration purposes because it is principally a 511-keV γ-ray emitter from positron annihilation within the source and its housing. Because the NaI crystal sensitivity depends on the position and the angle of the incoming γ ray, one of

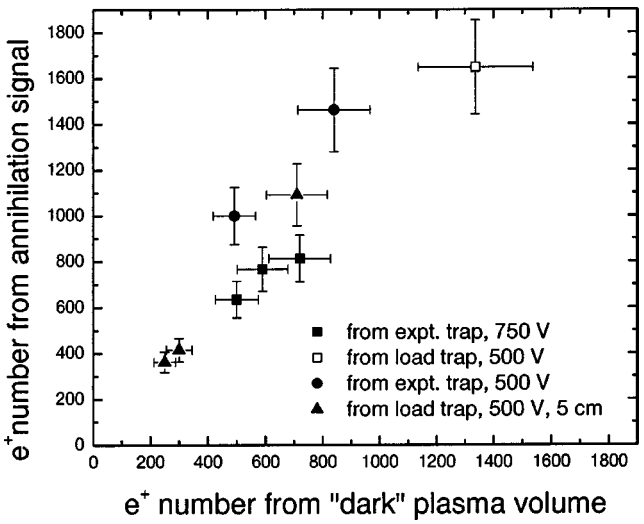

FIG. 3. Comparison of the number of trapped positrons obtained from the calibrated annihilation signal with the number obtained from the volume and density of the ''dark'' plasma column. Positrons were ejected from the load or the experimental trap, with different voltage pulse heights (500 V, 750 V), and with the NaI crystal located 2.5 cm (squares and circles) and 5 cm (triangles) from the Ti foil. The NaI crystal detection system was calibrated with a 32.9 kBq (~ 1 μCi) ^{68}Ge source.

the larger uncertainties in the calibration is due to the difference in the size of the ^{68}Ge 511-keV γ-ray source (~ 5 mm active diameter) and the annihilation spot on the Ti foil (<1 mm diameter). Overall we estimate the uncertainty in determining the number of annihilated positrons from the peak of the preamplifier output pulse to be $\sim 25\%$.

Figure 3 compares the number of positrons determined from the annihilation signal with the number of positrons calculated from the volume and density of the dark central column (before annihilation). We assume a positron density given by a rigid rotation of the positrons with the ^{9}Be^{+} ions, and that the column consists of positrons only. The different symbols correspond to the results obtained with the plasma ejected from either the load or experimental trap and with different voltage pulse heights. Some systematic variation between the different procedures is observed. While we do not understand this variation, the positron number determined by the annihilation method should produce a lower limit for the number of trapped positrons. In fact in all cases, Fig. 3 indicates a slightly larger annihilation signal than expected from the measured volume of the light-mass column. However, the difference is only of the order of the estimated systematic uncertainty of the measurements (25% for the calibration of the annihilation signal and 30% for the volume estimate).

The annihilation measurements support the conclusions reached with the lifetime measurements, i.e., the light-mass charges observed in the centrifugal separation are positrons. In addition, the number and density of the positrons is consistent with an approximate rigid rotation of the positrons with the ^{9}Be^{+} ions. Evidently, the momentum transfer between the ^{9}Be^{+} ions and positrons is sufficient to overcome any ambient torques on the positrons which oppose the rotation. Sources of such torque include trap construction errors and the coupling of the positrons to the stationary background radiation field [32].

We observed centrifugal separation of the positrons with rotation frequencies up to 1 MHz. For larger rotation frequencies, the radius of the positron column was too small to clearly see separation. In the 6 T magnetic field of this experiment, $\omega_R \approx 2\pi \times 1$ MHz gives a positron density $\geqslant 4\times 10^{9}$ cm^{-3}, which is ~ 50 times greater than the highest positron density previously achieved [14].

IV. POSITRON ACCUMULATION

Our positron accumulation rate was low ($\lesssim 50$ positrons per hour) and limited the total number of trapped positrons to ~ 2000. Two different schemes for loading positrons were explored. First we attempted to mimic the procedure of Gabrielse and co-workers of field ionizing Rydberg positronium formed as the moderated positrons leave the moderator crystal [11,12].

The basic idea of the field-ionization technique is that in a high magnetic field, a fraction of the moderated positrons that leave the moderator crystal combine with an electron to form positronium in a very high Rydberg state. The positronium then travels into the trap as long as the electric fields between the moderator and trap are not large enough to field ionize the Rydberg state. The trap potentials are adjusted to give a larger electric field inside the trap capable of field ionizing the positronium and therefore capturing the positron. Figure 4 shows an example of the on-axis potential and electric field we used in our attempt to accumulate positrons via field ionization of Rydberg positronium. Positrons were accumulated with a number of different overall well depths (or electric-field strengths) while maintaining roughly the same trap potential shape.

Figure 5 shows the accumulation of positrons for two different trap depths. The solid curves are fits to the rate equation $dN/dt = a - N/\tau$ for the number of accumulated positrons N. The fitted accumulation rates a are listed in the figure. For both datasets, the fitted $1/e$ lifetime τ was ~ 120 h. This is a significantly shorter lifetime than that measured in Fig. 2 where the ^{22}Na source was removed and voltages symmetric about the trap center were applied to the experimental trap electrodes. Similar to Ref. [11], we observed an increase in the number of accumulated positrons as the maximum electric-field strength within the trap was increased. However, our maximum accumulation rate (trap voltage ~ 200 V) occurs at an electric-field strength that is of the order of ten times greater than that observed in Ref. [11]. The observed loading efficiency was $\sim 10^{3}$ times less than that observed in Refs. [11,12] and is likely explained by the sensitivity of this technique to an absorbed gas layer on the moderator crystal. Gabrielse and co-workers used a cryogenic tungsten moderator and observed a decrease in efficiency if the moderator was heated after cooling to 4 K. We used a room-temperature Cu moderator that was baked to 350 °C during the vacuum bakeout. Therefore our moderator crystal was not expected to have the same absorbed gas layer as in the experiment of Gabrielse and co-workers.

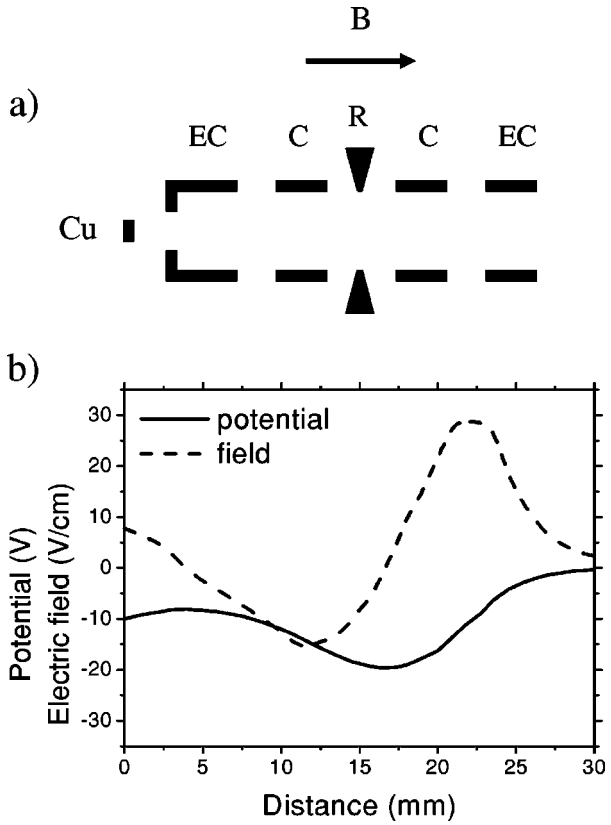

FIG. 4. (a) Schematic diagram of the experimental Penning trap and (b) the calculated on-axis potential well and electric fields for $-10,-8,-8,-17,-25,-22$ V on the Cu crystal and trap electrodes, from left to right. The adjacent load trap electrodes were at 0 V. This was one of the smaller well depths used to accumulate positrons.

We also investigated positron loading through Coulomb collisions with laser-cooled $^9Be^+$ ions. Calculations indicate that this technique can efficiently trap positrons [18]. For example, with a 2-mCi source, calculations indicate that this technique can trap positrons at a rate of $\sim 20\ s^{-1}$, assuming a moderator efficiency of 10^{-3} and a 300-K distribution of moderated positrons passing through a 10^{10}-cm^{-3} $^9Be^+$ plasma of 1 cm length. This requires $\sim 10^8$ $^9Be^+$ ions for complete overlap with the 1-mm-diameter positron source. Because this technique's efficiency depends on the energy distribution of the moderated positrons, before accumulating positrons, we cleaned and annealed the Cu moderator crystal by (*in situ*) electron bombardment heating to $\sim 800\,°C$ for ~ 30 min. Figure 6 shows the positron accumulation rate as a function of the bias of the Cu moderator crystal relative to the experimental trap lower end cap. The accumulation rate rises rapidly over a few tenths of a volt near -1 V. However, for a room-temperature distribution of moderated positrons, an order of magnitude sharper increase in the positron accumulation rate is anticipated.

To compare our measured accumulation rate with the calculations in Ref. [18], the dependence of the accumulation rate on the $^9Be^+$ plasma size and on the energy distribution of the moderated positrons must be taken into account. The largest $^9Be^+$ plasmas we could routinely load and cool in this trap were $\sim 10^6$ ions. From scaling factors calculated in Ref. [18], we estimate that this reduces the positron loading efficiency from the bench mark calculation with 10^8 ions by a factor of 80. A spread of a few tenths of a volt in the axial energy of the moderated positrons will also result in a factor of ~ 100 decrease in loading efficiency over that obtained with a room-temperature spread. Just these two factors can account for our low accumulation rate. However, because we do not have independent measurements of the moderator crystal efficiency and the energy spread of the moderated

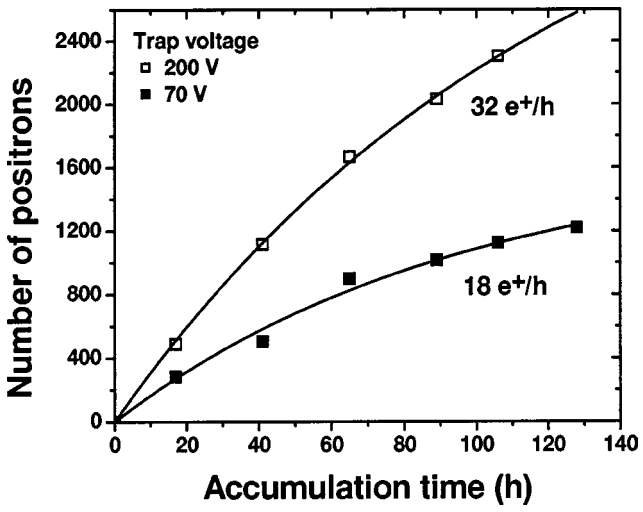

FIG. 5. Number of positrons vs accumulation time for two different trap depths. The 200-V trap corresponds to $-40,-38,-200,-220,-200$, 0 V and the 70-V trap to $-15,-13,-70,-77,-70$, 0 V on the moderator crystal and experimental trap electrodes. Here the potential of the moderator crystal is listed first followed by the experimental trap electrode potentials in order of their proximity to the moderator crystal.

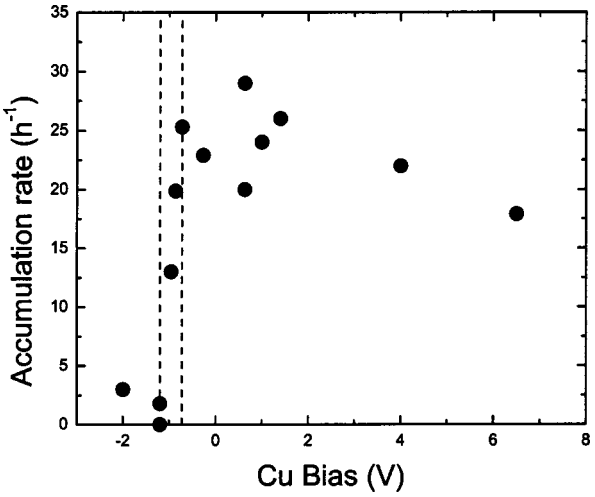

FIG. 6. Positron accumulation rate, obtained while attempting to load through Coulomb collisions with laser-cooled $^9Be^+$ ions (and sympathetically cooled e^+), vs the moderator crystal bias. Typical plasmas consisted of $\sim 10^6$ $^9Be^+$ ions with ≈ 500 positrons. The dashed vertical lines indicate a 0.5-V interval over which the positron accumulation rate rapidly increases to its maximum value.

positrons, we cannot determine whether the accumulation rate in Fig. 6 is due to Coulomb collisions.

V. POSITRON TEMPERATURE

With sympathetic laser cooling, the positron temperature can, in principle, be as cold as the $^9Be^+$ temperature. That is, positron temperatures of the order of 10 mK, where the positrons form a crystal [7], are possible. Unfortunately, there are no easy methods for measuring positron temperatures this low. We investigated two different methods for obtaining information on the positron temperature: (1) spectroscopy on the positron cyclotron resonance and (2) the sharpness of the centrifugal separation. While the spectroscopic information on the cyclotron resonance was dominated by effects other than temperature, an upper limit on the positron temperature $T_{\|}(e^+)$ of motion parallel to the magnetic field was extracted from the sharpness of the centrifugal separation. The two methods are discussed below.

A. Positron cyclotron resonance

In a magnetic field of 6 T, the positron cyclotron resonance occurs at a frequency of $\sim$166 GHz. The positron cyclotron resonance will be shifted and broadened by the relativistic mass shift ($\sim$12.6 kHz for room-temperature positrons) and possibly broadened by first-order Doppler shifts due to the axial motion of the positrons. We generated microwaves at 166 GHz by tripling the output of a $\sim$50 mW klystron at 55 GHz. For the resonance curve in Fig. 7(a), the output of the klystron was attenuated by $\sim$20 dB. A multimode waveguide carried the 166-GHz microwave radiation into the magnet bore close to the trap center. No special care was used in coupling the microwaves into the trap. Microwaves that leaked out of the end of the waveguide had to pass through the quartz vacuum envelope and between the gaps in the trap electrodes in order to excite the positron cyclotron motion. Excitation of the positron cyclotron motion increases the positron energy. Through the Coulomb interaction the positrons then increase the $^9Be^+$ ion energy, which changes the level of the $^9Be^+$ ion resonance fluorescence.

Figure 7(a) shows the change in the $^9Be^+$ resonance fluorescence as the frequency of the microwaves is stepped across the positron cyclotron resonance. The 200-kHz width is larger by more than an order of magnitude than the largest anticipated relativistic mass shifts ($\sim$12 kHz for a 300-K positron). First-order Doppler shifts can be much larger. For example, a 1-K positron moving along the z (axial) direction produces a Doppler shift of $\sim$2 MHz in the positron cyclotron resonance for microwaves traveling along the same direction. For our experiment though, Fig. 1(b) shows that the positrons are confined to a volume with characteristic dimension much less than than the 1.8 mm wavelength of the 166-GHz microwaves. In this Lamb-Dicke limit, first-order Doppler broadening will take place as sidebands instead of contributing to the resonance width of Fig. 7(a). Broadening due to magnetic-field instability and inhomogeneity is expected to be at most a few kilohertz.

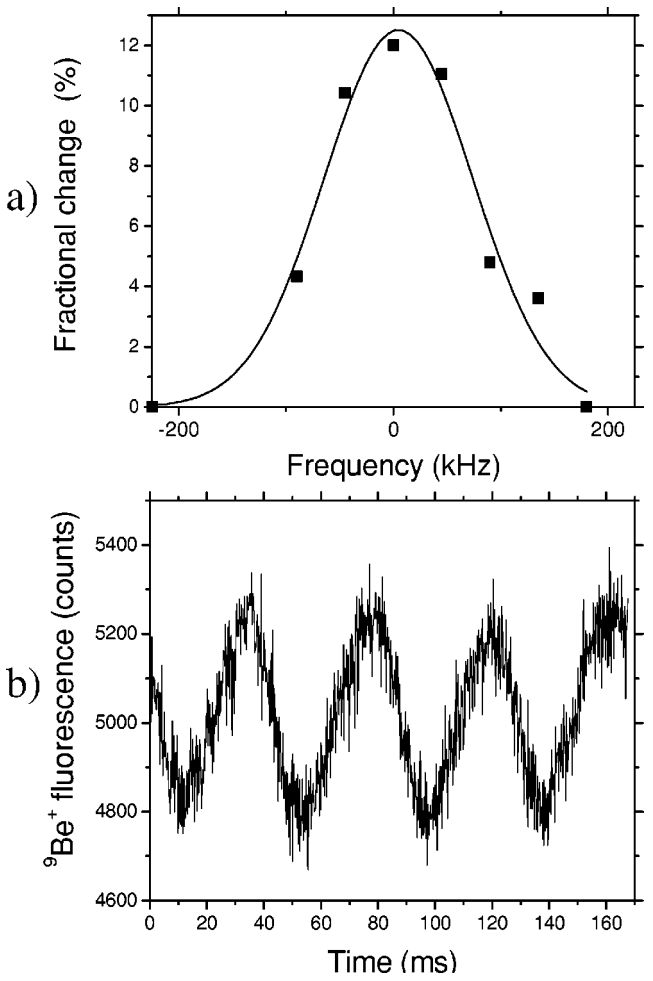

FIG. 7. Positron cyclotron resonance. (a) Resonance curve recorded at low microwave power. The frequency scale is the applied microwave frequency minus 165 857 083.5 kHz. (b) $^9Be^+$ fluorescence signal when the amplitude of the applied microwaves is chopped at 22 Hz. The curve in (a) is a fit to a Gaussian through the data points obtained by measuring peak-to-peak values of (b). For each frequency, the data in (b) were averaged on a multichannel scaler for >5 min.

We believe that the $\sim$200 kHz resonance width of Fig. 7(a) was probably caused by power broadening. When increasing the microwave power from a low value, a sharp threshold in the power needed to observe the resonance was observed. Figure 7 was recorded slightly above this threshold. An increase of only $\sim$5 dB in the applied microwave power above this threshold was sufficient to rapidly annihilate the positrons, presumably through excitation of the positrons to at least a few eV where positronium formation with background gas atoms could take place. The apparent significant excitation of the positron cyclotron motion that was required to observe the resonance was probably necessary because of the weak coupling between the positron cyclotron motion and the $^9Be^+$ ion and positron axial motions. For example, experimental and theoretical studies [33] have shown that in large magnetic fields, the energy equipartition rate between the positron cyclotron and axial motions becomes exponentially weak in the limit of low temperature.

This point is discussed more completely below.

In an attempt to obtain temperature information from first-order Doppler effects, we also searched for sidebands near the plasma frequency ($\sim$200–500 MHz) of the positrons, but did not observe any. In fact, because of the large plasma frequency, we expect that axial sidebands will be observable only at significant temperatures ($\gtrsim$300 K). We were also unable to observe any sidebands due to the plasma rotation.

B. Centrifugal separation

Because we could not find a more direct method, we used the centrifugal separation of the $^9Be^+$ ions and positrons to place an upper limit on $T_\parallel(e^+)$. In the 6 T magnetic field, the positron cyclotron radius becomes smaller than the distance of closest approach for temperatures $\lesssim$100 K. In this strongly magnetized regime the positron cyclotron motion decouples from the other degrees of freedom, with the result that the distribution function for the positrons is determined by $T_\parallel(e^+)$ and not $T_\perp(e^+)$ [34]. $T_\parallel(e^+)$ will be cooled sympathetically through the Coulomb interaction with the laser-cooled $^9Be^+$ ions. However, we expect this cooling to be weak because of the large difference in the positron and $^9Be^+$ masses and because of the small overlap of the species due to the centrifugal separation. Due to this weak coupling, $T_\parallel(e^+)$ could be larger than the $^9Be^+$ temperature. Therefore, we calculated the positron and $^9Be^+$ density profiles assuming zero-temperature $^9Be^+$ ions $[T_\parallel(^9Be^+) = T_\perp(^9Be^+) = 0]$ but nonzero-temperature positrons $[T_\parallel(e^+) > 0]$. Even though we do not assume equal temperatures, we do assume rotational equilibrium of the positron and $^9Be^+$ ions. This is experimentally supported by our positron detection measurements (Sec. III).

The calculation closely follows the profile calculations discussed in Refs. [19,35] for an infinitely long plasma column. Figure 8 shows the results of these calculations (positron and $^9Be^+$ ion relative density profiles) for two different temperatures ($T = 0.5$ and 3 K) and for conditions similar to some of the experimental measurements ($\omega_r = 2\pi \times 500$ kHz, N_L = number of positrons/length $= 1.5 \times 10^5$ cm^{-1}) [36]. For a given $T_\parallel(e^+)$, the $^9Be^+$ density makes a sharp jump from zero density at a radius determined primarily by the value of N_L. This jump is then followed by a gradual increase at larger radii. As $T_\parallel(e^+)$ increases, the sharp jump becomes smaller and the subsequent increase in the $^9Be^+$ density more gradual. In the experimental measurements, the plasma axial extent was typically smaller than the overall plasma diameter [see Fig. 1(b)]. However, the calculations should correctly describe the separation of the species as long as the diameter of the dark region in the $^9Be^+$ fluorescence is of the same order of, or smaller than, the axial extent of the plasma. We typically worked in this regime.

An experimentally measured profile of the $^9Be^+$ ion fluorescence, assumed to be proportional to the ion density, is shown in Fig. 9(a). The plasma rotation frequency was $\omega_r = 2\pi \times 500$ kHz, which gives $n_{e^+} \simeq n_{Be^+} = 2 \times 10^9$ cm^{-3}. It contained 1.3×10^5 $^9Be^+$ ions and $\sim$1700 positrons. Also

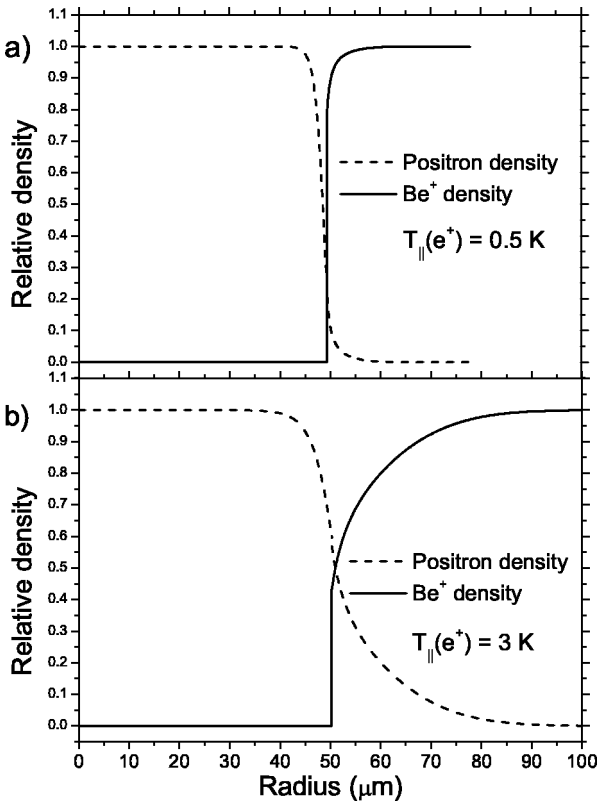

FIG. 8. Calculated radial variation of positron and $^9Be^+$ ion densities for an infinitely long column with cold $^9Be^+$ ions $[T_\parallel(^9Be^+) = T_\perp(^9Be^+) = 0]$ but for different positron temperatures. (a) $T_\parallel(e^+) = 0.5$ K, (b) $T_\parallel(e^+) = 3$ K.

shown in Fig. 9(a) is the measured $^9Be^+$ fluorescence profile in a plasma consisting of $^9Be^+$ ions and impurity ions of light mass created by ionizing background gas molecules. Note that both profiles are nearly identical. They both show small but nonzero fluorescence for $r \leqslant 20$ μm and a gradual, nearly identical rise in fluorescence at $r \sim 50$ μm. The offset in fluorescence is due to the size of the laser beam waist ($\sim$50 μm) compared to the diameter of the nonfluorescing column ($\sim$100 μm). From previous studies of sympathetic cooling [17–20], we expect the temperature of both the $^9Be^+$ ions and impurity ions to be $\lesssim$0.5 K and therefore expect a sharp increase in the $^9Be^+$ density such as that shown in Fig. 8(a). We believe that the much more gradual increase in the $^9Be^+$ fluorescence observed in Fig. 9(a) is due to the resolution of the side-view imaging system. Figure 9(a) is consistent with an instantaneous rise of the $^9Be^+$ density at the boundary between the impurity and the $^9Be^+$ ions, convoluted with a Gaussian response function of 28-μm full width at half maximum (FWHM). This resolution is about three times worse than that expected from a different experiment, which also used $f/5$ optics [37], and is probably due to astigmatism produced by viewing through a vacuum window at an 11° angle of incidence.

Figure 9(b) compares the measured $^9Be^+$ fluorescence profile (obtained with positrons) in Fig. 9(a) with the expected $^9Be^+$ fluorescence profile for $T_\parallel(e^+) = 3$ K. The expected $^9Be^+$ fluorescence profile was obtained by convolut-

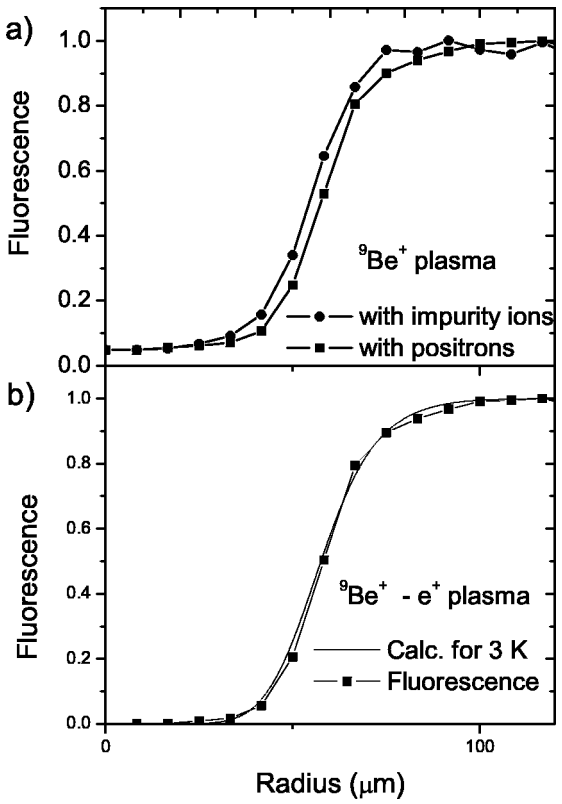

FIG. 9. (a) Measured radial dependence of the $^9Be^+$ fluorescence for a $^9Be^+$ impurity ion plasma and for a $^9Be^+$-e^+ plasma. (b) $^9Be^+$-e^+ plasma fluorescence curve shown in (a) compared with a calculated curve of the $^9Be^+$ fluorescence for $T_\parallel(e^+)=3$ K. The nonzero fluorescence at $r=0$ in (a) has been subtracted. The calculated curve was obtained by convoluting the $^9Be^+$ density curve of Fig. 8(b) with a 28-μm FWHM Gaussian response of the side-view imaging system.

ing the calculated density profile for $T_\parallel(e^+)=3$ K (see Fig. 8) with the estimated 28-μm Gaussian response function of the image detection system. Good agreement is observed between the two curves. This indicates that $T_\parallel(e^+)\lesssim 3$ K. However, this limit depends sensitively on the estimated response function of the image detection system. Because we do not have a truly independent measure of this response function, we place a conservative limit of $T_\parallel(e^+)\lesssim 5$ K by directly comparing the profiles in Fig. 9(a) with calculations such as those shown in Fig. 8.

We were not able to place any experimental limits on $T_\perp(e^+)$. We know that the positron cyclotron motion was radiatively coupled to the room-temperature walls of the trap with a free space decay rate of 13.6 s^{-1}. The positron cyclotron motion was also coupled by collisions with the positron motion parallel to the magnetic field. This coupling, which has been well studied both theoretically and experimentally [33], becomes exponentially weak for low-temperature positron (or electron) plasmas in high magnetic field. Specifically, the positron $T_\perp/T_\parallel$ collisional equipartition rate ν scales as $\exp[-5(3\pi\kappa)^{2/5}/b]$ for $\kappa\equiv(b/r_c)/\sqrt{2}$. Here b is the classical distance of closest approach and r_c is the thermally excited cyclotron radius. For a 2×10^9 cm^{-3} positron plasma, ν is greater than 13.6 s^{-1} for $T_\perp(e^+)\sim T_\parallel(e^+)\gtrsim 10$ K, but decreases exponentially as the temperature is reduced. Therefore as the $^9Be^+$ ions sympathetically cool $T_\parallel(e^+)$, we anticipate $T_\perp(e^+)\sim T_\parallel(e^+)$ for $T_\parallel(e^+)\gtrsim 10$ K. As $T_\parallel(e^+)$ is cooled to lower temperatures, the radiative coupling of the positron cyclotron motion prevents further cooling of $T_\perp(e^+)$. The equipartition rate ν has not been studied for large differences between $T_\parallel$ and $T_\perp$. However, due to its exponential dependence on the distance of closest approach, the $T_\perp/T_\parallel$ equipartition rate could be significantly reduced as $T_\parallel(e^+)$ is cooled below 10 K. This means that $T_\perp(e^+)$ could increase as $T_\parallel(e^+)$ is cooled below 10 K. Without further estimates of the equipartition rate for the case of large differences between $T_\perp(e^+)$ and $T_\parallel(e^+)$, we can place only the $10\text{ K}\lesssim T_\perp(e^+)\lesssim 300$ K limits on $T_\perp(e^+)$.

VI. SUMMARY

In summary, we have demonstrated sympathetic cooling and compression of small numbers ($\sim$2000) of positrons with laser-cooled $^9Be^+$ ions. The observed centrifugal separation implies that the positrons and $^9Be^+$ ions rotate rigidly and have comparable densities, indicating positron densities of $\gtrsim 4\times10^9$ cm^{-3}. This is $\sim$50 times greater than the highest positron density previously achieved [14] and could be useful in experiments making antihydrogen. The positron lifetime is greater than two weeks in our room-temperature trap. We use the sharpness of the centrifugal separation to place a conservative upper limit of 5 K on the positron temperature for motion parallel to the magnetic field.

The low accumulation rate limited the number of positrons that could be accumulated to a few thousand. This number needs to be significantly increased for most of the potential applications of cold positrons. This could be done by combining the sympathetic cooling technique with an established technique for accumulating positrons [11–14]. It is interesting to speculate about the maximum number of positrons that can be sympathetically cooled. A potential limit is the number of ions that can be directly laser cooled. We can routinely load and laser cool $\sim10^6$ $^9Be^+$ ions to temperatures $\lesssim 10$ mK. This ion number is limited by our loading technique rather than by the capabilities of laser cooling. With a different loading technique, non-neutral plasmas of $\sim10^9$ Mg^+ ions have been laser cooled to temperatures of $\sim$1 K [38]. Therefore it may be feasible to sympathetically laser cool $\sim10^9$ positrons, comparable to the largest number of positrons that have been trapped in a Penning-Malmberg trap. This would provide a useful, very cold source of positrons in a room-temperature vacuum system.

ACKNOWLEDGMENTS

This work was supported by the Office of Naval Research. We acknowledge useful discussions with T. M. O'Neil and D. J. Wineland. We also thank B. Zimmerman and B. Coursey at the NIST Ionizing Radiation Division for the calibration of the activity of the ^{68}Ge source. One of us (B.M.J.) thanks MNTS (Serbia), Project No. 1443 for financial assistance.

[1] P.J. Schultz and K.G. Lynn, Rev. Mod. Phys. **60**, 701 (1988).
[2] W.E. Kauppila and T.S. Stein, Adv. At., Mol., Opt. Phys. **26**, 1 (1990).
[3] S.J. Gilbert, L.D. Barnes, J.P. Sullivan, and C.M. Surko, Phys. Rev. Lett. **88**, 043201 (2002).
[4] The ATHENA Collaboration, M. Amoretti, Nature (London) **419**, 456 (2002).
[5] The ATRAP Collaboration, G. Gabrielse, Phys. Rev. Lett. **89**, 213401 (2002).
[6] R.G. Greaves and C.M. Surko, Phys. Rev. Lett. **75**, 3846 (1995).
[7] J.H. Malmberg and T.M. O'Neil, Phys. Rev. Lett. **39**, 1333 (1977).
[8] P.B. Schwinberg, R.S. Van Dyck, Jr., and H.G. Dehmelt, Phys. Lett. **81A**, 119 (1981).
[9] R.S. Conti, B. Ghaffari, and T.D. Steiger, Nucl. Instrum. Methods Phys. Res. A **299**, 420 (1990).
[10] H. Boehmer, M. Adams, and N. Rynn, Phys. Plasmas **2**, 4369 (1995).
[11] J. Estrada *et al.*, Phys. Rev. Lett. **84**, 859 (2000).
[12] The ATRAP Collaboration, G. Gabrielse, Phys. Lett. B **507**, 1 (2001).
[13] C.M. Surko, S.J. Gilbert, and R.G. Greaves, in *Non-Neutral Plasma Physics III*, edited by J. Bollinger, R. Spencer, and R. Davidson (AIP, Melville, NY, 1999), p. 3.
[14] R.G. Greaves and C.M. Surko, Phys. Rev. Lett. **85**, 1883 (2000).
[15] B.M. Jelenković *et al*, in *New Directions in Antimatter Chemistry and Physics*, edited by C.M. Surko and F.A. Gianturco (Kluwer Academic, The Netherlands, 2001), pp. 1–20.
[16] B.M. Jelenković *et al.*, Nucl. Instrum. Methods Phys. Res. B **192**, 117 (2002).
[17] D.J. Wineland, C. Weimer, and J.J. Bollinger, Hyperfine Interact. **76**, 115 (1993).
[18] A.S. Newbury, B.M. Jelenković, J.J. Bollinger, and D.J. Wineland, Phys. Rev. A **62**, 023405 (2000).
[19] T.M. O'Neil, Phys. Fluids **24**, 1447 (1981).
[20] D.J. Larson *et al.*, Phys. Rev. Lett. **57**, 70 (1986).
[21] J.J. Bollinger *et al.*, IEEE Trans. Instrum. Meas. **40**, 126 (1991).
[22] H. Imajo *et al.*, Phys. Rev. A **55**, 1276 (1997).
[23] L. Gruber *et al.*, Phys. Rev. Lett. **86**, 636 (2001).
[24] D.S. Hall and G. Gabrielse, Phys. Rev. Lett. **77**, 1962 (1996).
[25] D.J. Heinzen *et al.*, Phys. Rev. Lett. **66**, 2080 (1991).
[26] X.-P. Huang, J.J. Bollinger, T.B. Mitchell, and W.M. Itano, Phys. Plasmas **5**, 1656 (1998).
[27] L.R. Brewer *et al.*, Phys. Rev. A **38**, 859 (1988).
[28] C.A. Murray and A.P. Mills, Jr., Solid State Commun. **34**, 789 (1980).
[29] R.J. Wilson, Phys. Rev. B **27**, 6974 (1983).
[30] Previous Refs. [15,16] listed a positron lifetime of 200 h. This lifetime was extracted from a fit of the data in Fig. 2 to an exponential plus a constant offset. The correct lifetime (360 h) is obtained by fixing the offset to be zero.
[31] S.J. Gilbert, C. Kurz, R.G. Greaves, and C.M. Surko, Appl. Phys. Lett. **70**, 1944 (1997).
[32] T.M. O'Neil, Phys. Fluids **23**, 725 (1980).
[33] M.E. Glinski, T.M. O'Neil, and M.N. Rosenbluth, Phys. Fluids B **4**, 1156 (1992).
[34] D.H.E. Dubin and T.M. O'Neil, Phys. Rev. Lett. **60**, 511 (1988).
[35] D.H.E. Dubin and T.M. O'Neil, Rev. Mod. Phys. **71**, 87 (1999).
[36] Profile calculations prevously published in Refs. [15,16] contained a slight error. This did not change our estimated limit on $T_{\|}(e^+)$.
[37] T.B. Mitchell, J.J. Bollinger, W.M. Itano, and D.H.E. Dubin, Phys. Rev. Lett. **87**, 183001 (2001).
[38] E.M. Hollmann, F. Anderegg, and C.F. Driscoll, Phys. Rev. Lett. **82**, 4839 (1999).